

ASTRAEA: A GPU-Oriented Token-wise Acceleration Framework for Video Diffusion Transformers

Haosong Liu^{1*} Yuge Cheng^{1*} Zihan Liu¹ Aiyue Chen² Jing Lin² Yiwu Yao²
Chen Chen¹ Jingwen Leng^{1,2} Yu Feng^{1,2,#} Minyi Guo^{1,2}

¹Shanghai Jiao Tong University ²Shanghai Qizhi Institute ³Huawei Technologies Co.,Ltd

*Equal Contribution #Corresponding Author

{2436824987, chengyuge, altair.liu, chen-chen, leng-jw, y-feng}@sjtu.edu.cn
guo-my@cs.sjtu.edu.cn

{chenaiyue, linjing28, yaoyiwu}@huawei.com

Project site: <https://astraea-project.github.io/ASTRAEA/>

Abstract

Video diffusion transformers (vDiTs) have made impressive progress in text-to-video generation, but their high computational demands present major challenges for practical deployment. While existing acceleration methods reduce workload at various granularities, they often rely on heuristics, limiting their applicability.

We introduce ASTRAEA, an automatic framework that searches for near-optimal configurations for vDiT-based video generation. At its core, ASTRAEA proposes a lightweight token selection mechanism and a memory-efficient, GPU-parallel sparse attention strategy, enabling linear reductions in execution time with minimal impact on generation quality. To determine optimal token reduction for different timesteps, we further design a search framework that leverages a classic evolutionary algorithm to automatically determine the distribution of the token budget effectively. Together, ASTRAEA achieves up to $2.4\times$ inference speedup on a single GPU with great scalability (up to $13.2\times$ speedup on 8 GPUs) while retaining better video quality compared to the state-of-the-art methods ($<0.5\%$ loss on the VBench score compared to the baseline vDiT models).

1 Introduction

Visual imagination has always been at the core of humanity’s nature for creativity. After the release of Sora by OpenAI in early [3], there are numerous video generative frameworks from text input, including SenseTime’s Kling [2], Google’s Veo [4], and Tencent’s Hunyuan [1].

Despite the abundance of frameworks, video diffusion transformers (vDiTs) remain the core of these frameworks, widely regarded as the most effective paradigm due to its ability to generate high-fidelity videos. However, its computational demand poses a significant challenge for any industrial-level deployment. For instance, a 4-second 720×1280 video clip on a Nvidia H100 GPU takes over 0.5 hours using Hunyuan [20]. This high computational cost comes from the *extensive denoising steps* and the *large number of tokens*. For example, a vDiT model often requires 50-100 denoising steps, with each step involving over millions of tokens.

Various acceleration methods have been proposed to reduce computational workload at different granularities, such as denoising step reduction [21, 35, 14], intermediate block caching [40, 8, 18, 13], token selection [43], etc. However, these methods often require iteratively fine-tuning hyperparameters, i.e., which steps or blocks to skip, with a human in the loop to achieve a target performance in industrial-level deployments. Fundamentally, previous approaches primarily propose various acceleration heuristics, without addressing a key question: *given a specific performance target, which tokens are worth computing at each denoising step to achieve optimal accuracy?*

Preprint.

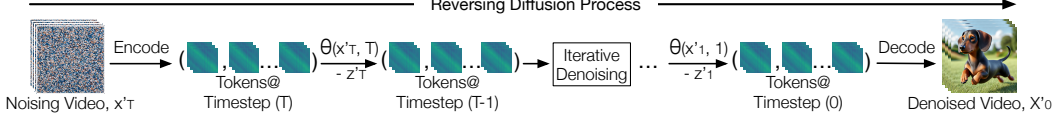


Fig. 1: Diffusion models work by reversing a diffusion process, where they iteratively predict and remove noise at each timestep to gradually reconstruct the original images or videos.

To answer this question, we propose ASTRAEA, a GPU-friendly acceleration framework that operates at the token level, the smallest primitive in vDiT models. Specifically, we propose a sparse diffusion inference with a lightweight token selection mechanism and GPU-efficient sparse attention to accelerate each denoising step by dynamically selecting important tokens. To determine optimal token budget allocation, we propose a search framework that determines the number of tokens that should be assigned in each denoising step to achieve the target performance.

Algorithm. Our selection mechanism is largely aware of the extensive GPU memory usage in prior work [43]. Unlike prior studies, which require storing the entire attention map, our mechanism introduces negligible memory overhead by only caching previous token values. Thus, the memory requirement of our selection metric scales sub-linearly with the token length to avoid a memory explosion. In addition, we purposely design our sparse attention to be natively parallelizable, thus, it can be integrated with existing attention acceleration techniques, such as FlashAttention [11, 10]. On existing GPUs, our sparse attention achieves linear execution delay with the number of input tokens.

Search Framework. Although our algorithm can achieve linear acceleration for each denoising timestep, it is still unknown how many tokens should be allocated for individual timesteps. While numerous search techniques exist in the literature, such as neural architecture search [30, 12] and network pruning [16, 9], none can be applied to vDiTs due to their substantial search times. Here, we propose a search framework based on the classic evolutionary search algorithms [31, 5]. Our approach guarantees to achieve the target performance while achieving the minimal accuracy loss.

Compared to the state-of-the-art algorithms, ASTRAEA achieves up to $2.4\times$ speedup with better generation quality (less than 0.5% loss on VBench score). Also, ASTRAEA easily scales to $13.2\times$ speedup across 8 GPUs. Our contributions are summarized as follows:

- We propose a lightweight token selection mechanism to reduce the computation workload of each denoising step with negligible latency and memory overhead.
- We design a sparse attention computation method that achieves linear speedup on existing GPUs, as the number of selected tokens decreases.
- We introduce a search framework that meets the target performance while achieving the minimal accuracy loss against prior studies.

2 Related Work

Diffusion models have been widely used in video generation. It learns to generate data from Gaussian noise through a reverse Markov process (Fig. 1). The input of this diffusion process is a randomly generated Gaussian noise, x'_T . The diffusion model recovers the original data by progressively predicting and removing noise, z'_t , from x'_t at each timestep t . The hope is that, through this process, the prediction of the diffusion model, x'_0 , can be close to the original data, x_0 . Mathematically, the denoising step can be expressed as,

$$x'_{t-1} = \alpha_t(x'_t - \beta_t z'_t) + \sigma_t n'_t, \quad z'_t = \Phi(x'_t, t), \quad (1)$$

where Φ is the prediction function that predicts the noise z'_t . Both α_t and β_t are hyper-parameters. $\sigma_t n'_t$ is the renoising term to add randomness to the denoising step.

Normally, diffusion models often require hundreds or even thousands of steps to denoise images or videos [34]. The common practice to reduce the diffusion workload is to encode the initial noising inputs into the latent space then decode the tokens at the end, as shown in Fig. 1.

Prior methods to enhance the efficiency of diffusion models fall into two categories: *step reduction*, which reduces the number of denoising steps, and *block caching*, which seeks to minimize the computational demands within each denoising step. The following paragraphs overview these two categories of acceleration techniques separately.

Step Reduction. Overall, step reduction methods can be classified into two types: one requires retraining, and the other is training-free.

The retraining methods [35, 28, 14, 15, 19], such as distillation, can reduce the number of denoising steps to as few as one. However, the major downside of these methods is that they require as much training time as the original model training. For this reason, current distillation methods are primarily applied to image generation rather than video generation. For instance, Saliman et al. [28] propose progressive distillation that iteratively halves the number of required sampling steps by distilling a slow teacher diffusion model into a faster student model. BOOT [14] proposes a data-free distillation algorithm that learns a time-conditioned student model with bootstrapping objectives. DMD [35] uses a diffusion model to distill a one-step generator that can generate images with similar fidelities. Clockwork Diffusion [15] introduces a model-step distillation that enables asynchronous inference across different sub-models for efficient generation. BK-SDM [19] proposes a lightweight variant of Stable Diffusion optimized for fast, low-cost image generation with some performance degradation.

On the other hand, training-free methods do not require re-training and are generally less effective. The intuition of these training-free methods is to leverage the insignificance of predicted noises between steps, allowing diffusion models to skip these less critical steps. For instance, PAB [40] periodically skips two out of every three intermediate steps to reduce the overall computation. AutoDiffusion [21] applies heuristic search to iteratively develop better step-sampling strategies. FasterCache [25] reuses dynamic features and leverages CFG-guided caches for high-quality, accelerated video diffusion. Gradient-Optimized Cache [27] proposes a differentiable cache mechanism optimized via gradients to minimize reuse error. Fast Video Generation [39] introduces a tile-based attention pattern that accelerates video diffusion without requiring model retraining. AdaDiff [36] dynamically selects steps to skip during inference based on denoising difficulty, offering a fine-grained trade-off between speed and quality. Similar approaches [13] apply Taylor expansion to discard denoising steps.

Block Caching. The execution time of diffusion transformers is dominated by either 2D or 3D attention [22, 41]. To reduce the computation in self-attention, existing methods exploit the similarity of intermediate results across denoising steps and cache the intermediate results to avoid extra computations [40, 8, 18, 26, 32, 23, 24].

Primary caching methods operate at the block level. They reuse the computation result of a block from the previous denoising step and skip the corresponding block computation in the current denoising step entirely. The key difference among block-wise methods lies in the strategies they apply to reuse the intermediate results. For instance, PAB [40] applies a fixed step-skipping scheme throughout the entire inference process, whereas Δ -DiT [8] and AdaptiveCache [18] adopt an adaptive scheme to tailor the step reuse for each input. SmoothCache [24] proposes a universal caching mechanism that enables continuous reuse of transformer blocks via smooth temporal interpolation. Timestep Embedding Tells [23] introduces a step-aware caching strategy guided by timestep embeddings to improve caching efficiency in video diffusion models. BlockDance [37] exploits structural similarity across spatio-temporal blocks to enable coarse-grained caching. DiTFastAttn [38] performs head-wise attention compression to reduce computation cost in multi-modal diffusion transformers. Sparse VideoGen [33] exploits spatial-temporal sparsity to skip redundant computation in video diffusion without retraining. Both DeepCache [26] and Cache-Me-if-You-Can [32] are applied to UNet models. Nevertheless, the underlying concept remains unchanged.

Recently, few studies [43, 6] have started to explore reuse at a finer granularity, token level. For instance, ToCa [43] proposes a composed metric that identifies the unimportant tokens during the inference and uses the previously cached results for attention computation. However, its token selection process introduces non-trivial compute and memory overheads. Both are not affordable on modern GPUs. Due to the aforementioned reasons, token-wise methods are still not fully exploited and require careful algorithmic design to achieve actual speedup.

3 Methodology

3.1 Preliminary

Self-Attention. We first introduce one of the key operations in vDiTs: self-attention. The input to the self-attention, X_{in} , is a sequence of tokens with a shape of $\langle N, d \rangle$. N is the number of tokens

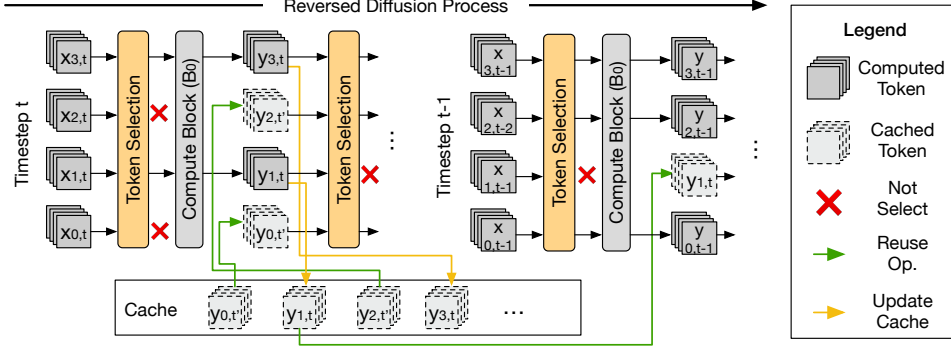


Fig. 2: The general diffusion process with selected tokens. For each compute block, a selection module determines which tokens should be computed. Only the selected tokens perform computation. The unselected tokens skip the computation block and query the cache for their results.

and d is the token channel dimension. The computation of self-attention can be expressed as,

$$\text{Attention}(Q, K, V) = \text{Softmax}\left(\frac{QK^T}{\sqrt{d_k}}\right)V, \quad (2)$$

where query Q , key K , and value V are generated by performing three independent linear projections on input tokens, X_{in} . These three values have the same dimensions as X_{in} . The product QK^T is commonly referred to as the attention map with a shape of $\langle N, N \rangle$. The attention map is then divided by $\sqrt{d_k}$ where d_k is the channel dimension of K . Finally, each row of the attention map, A_i , is normalized by the softmax function, where

$$\text{Softmax}(A_{i,j}) = \frac{e^{A_{i,j}}}{\sum_{k=1}^N e^{A_{i,k}}}, \quad (3)$$

before performing a dot product with V . i and j are the row and column indices of the attention map, A . Note that, $\sum_{k=1}^N e^{A_{i,k}}$ is often called the Log-Sum-Exp (LSE) score.

3.2 Token Selection

Execution Flow. Fig. 2 illustrates how our token selection integrates into the general diffusion process. For instance, at timestep t , there are four input tokens, $\langle x_{0,t}, \dots, x_{3,t} \rangle$. Before these tokens pass through a compute block (typically a stack of a self-attention layer, a cross-attention layer, and a multilayer perceptron in vDiTs), the token selection module first determines which tokens should be computed. Specifically, this module computes the importance of each token and selects the top important tokens, given a pre-defined computation budget, θ^* .

Tokens selected for computation are then processed through the compute block, and their outputs are used to update the cache. In contrast, unselected tokens would directly query their outputs from the cache, which stores results from the same compute block at earlier timesteps. The final output token sequence is a combination of both computed and cached tokens, e.g., $\langle y_{0,t'}, y_{1,t}, y_{2,t'}, y_{3,t} \rangle$ in Fig. 2. The same process is applied to all compute blocks in the subsequent diffusion process.

Selection Metric. Given the execution flow above, we next describe our token selection mechanism. The goal of token selection is to skip unimportant tokens while retaining the same generation quality. Despite studies [43, 7, 6] proposing various token selection mechanisms, they *either incur high computational and memory overhead* [43] *or are specifically tailored to particular tasks* [7, 6]. Thus, we propose a general token selection metric, S_{token} , that applies to all vDiTs.

Mathematically, S_{token} has two components,

$$S_{\text{token}} = w_{\alpha} S_{\text{sig}} + w_{\beta} S_{\text{penalty}}, \quad (4)$$

where S_{sig} stands for the significance of this token and S_{penalty} represents the penalty for repeatedly choosing the same token across multiple timesteps. Both w_{α} and w_{β} are the hyperparameters that are used to weigh the contributions of S_{sig} and S_{penalty} . S_{sig} is expressed as,

$$S_{\text{sig}} = S_{\text{LSE}} \Delta_{\text{token}}, \quad (5)$$

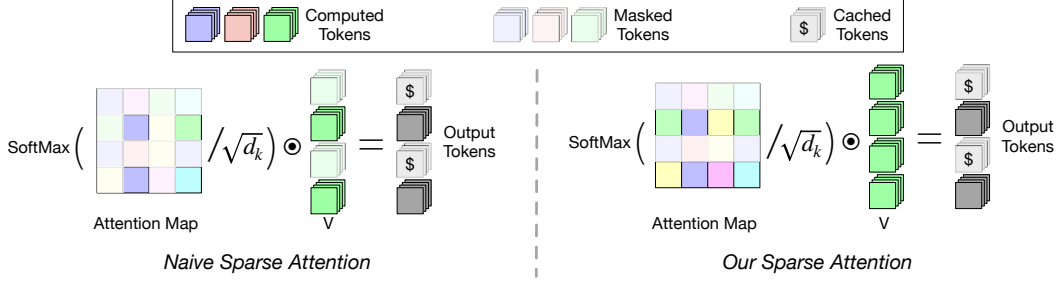


Fig. 3: An illustration of our sparse attention computation with selected tokens. While naive sparse attention reduces overall computation quadratically by computing the selected tokens on Q , K , and V , it suffers from computational inaccuracies and requires excessive memory usage. In contrast, our sparse attention only computes the selected tokens on Q and keeps all tokens for K and V .

where S_{LSE} is the LSE score of each token computed in the softmax function. Δ_{token} is the value difference of individual tokens across two adjacent computed timesteps. Here, the computed timestep means this token is computed at this timestep, instead of using the cached result. We include S_{LSE} in S_{sig} because its value is proportional to the attention score in self-attention, which reflects the token’s importance. Meanwhile, S_{LSE} is the byproduct of softmax and incurs no additional computational overhead. S_{penalty} can be expressed as,

$$S_{\text{penalty}} = e^{n_i}, \quad (6)$$

where n_i is the number of times the i th token has not been selected consecutively. This penalty term is inspired by ToCa [43], and we claim no contribution to this end.

Sparse Attention. Next, we describe how to perform vDiT inference with the selected tokens. There are three main computation operations in vDiT: self-attention, cross-attention, and multilayer perceptron (MLP) [41, 22]. Both cross-attention and MLP operate on individual tokens. To reduce the overall computation of cross-attention and MLP, we can directly skip the unselected tokens.

However, naively performing sparse self-attention with selected tokens, e.g., in ToCa [43], would result in accuracy loss. Because it alters the semantics of self-attention, as shown in Fig. 3. Only computing the unmasked positions in the attention map would lead to two issues: incorrect results and substantial memory overhead. This is because self-attention requires calculating the LSE score for each row in the attention map. Just computing the unmasked positions is semantically incorrect. Even using the results of the same attention in a previous denoising timestep would lead to accuracy loss. Meanwhile, it requires caching the entire attention map, which introduces high memory overhead. Tbl. 1 shows that our technique introduces much smaller memory overhead compared to prior work.

In contrast, we propose a seemingly “counterintuitive” sparse attention computation, as shown in Fig. 3, where we only selectively compute the queries Q while computing all tokens for the keys K and values V . Although this approach saves less computation than naive sparse attention, it offers the following advantages. First, by computing the entire row of elements in the attention map, we ensure the individual output token is computed correctly. Second, our sparse attention is natively GPU-parallelizable and can be integrated with existing attention acceleration techniques, such as FlashAttention [11]. Third, our sparse attention does not require any additional GPU memory, except for the cached tokens, which are negligible compared to the attention scores.

3.3 Token-wise Search Framework

Problem Setup. Sec. 3.2 explains how to select tokens of a compute block under a given token budget, θ^* . Naturally, the next question is what token budget should be assigned for each compute block. However, searching for token budgets at the compute block level would make the search space intractable. Thus, we fix the token budget at the timestep level and frame the problem as follows: *Given a total number of selected tokens, how should the token budget be allocated across timesteps?*

Search Space. In our framework, the search space is Θ , which can be expressed as,

$$\Theta = \{\theta_i\}, i \in [1, 2, \dots, T] \text{ and } \theta_i \in \{0, 0.1, 0.2, \dots, 1.0\}, \quad (7)$$

where θ_i is the percentage of selected tokens at the denoising timestep i . T is the maximal timestep.

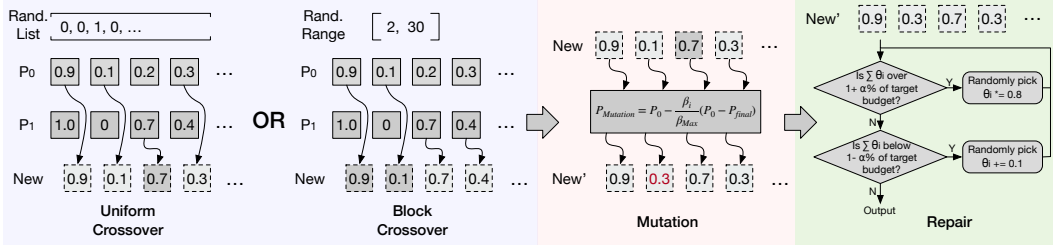


Fig. 4: An illustration of three key steps in EA. Each new candidate would go through these three steps sequentially before being added to the existing population. For each candidate, we would randomly pick from two crossover methods.

Algorithm. We now introduce our search algorithm. We adopt a classic stochastic search algorithm, evolutionary algorithm (EA) [31, 5], to search for the optimal token allocation across denoising steps. In standard EA, we start by spawning the initial generation of k candidates. Each candidate has a list of selected token percentages, $\{\theta_i\}_w$, that fits under the predefined token budget constraint, Θ_s .

At each generation, the top- k number of parents with smaller MSE losses are selected from the previous generation. We then generate P number of new candidates from this top- k parents. Each time, we randomly pick up a parent pair from the top- k parents. The selected parent pair then goes through three key steps: crossover, mutation, and repair, to generate new candidates. These newly generated candidates are added to the current population. These new candidates are then evaluated based on the MSE between the original video output and the output generated using the selected tokens. Finally, the top- k candidates with the lowest MSEs are selected for the next generation.

Next, we explain the procedure of these three key steps, as shown in Fig. 4.

Crossover. This step aims to generate a new candidate by combining two randomly picked candidates from the existing population. We propose two crossover strategies: *uniform crossover* and *block crossover*. Given two parent candidates, $\{\theta_i\}_{p0}$ and $\{\theta_i\}_{p1}$, uniform crossover randomly selects each θ_i from either parent with equal probability to form a new candidate. In contrast, block crossover first randomly creates a contiguous subset of timesteps within the range $[0, T]$. The new candidate then inherits all θ_i values within this subset from one parent, and the remaining values from the other parent. In the crossover step, we randomly pick between uniform crossover and block crossover.

Mutation. Once a new candidate $\{\theta_i\}_{\text{new}}$ is generated, the goal of mutation is to introduce a possibly better candidate by randomly mutating this candidate. Here, we decide whether each timestep would be mutated based on the probability,

$$P_{\text{mutation}} = P_0 - \frac{\beta_i}{\beta_{\text{Max}}}(P_0 - P_{\text{final}}), \quad (8)$$

where P_0 and P_{final} are the initial and the final probability of mutation, respectively. We find that gradually decreasing the mutation probability over generations leads to better convergence. β_i is the i th evolution generation and β_{max} is the maximal evolution generation. If a timestep were mutated, our algorithm would randomly change its θ_i from the valid value range, i.e., $\{0, 0.1, \dots, 1.0\}$.

Repair. A new candidate $\{\theta_i\}_{\text{new'}}$ from the previous two steps might no longer satisfy the token budget constraint, Θ_s . This repair step would ensure that the total token budget falls within the acceptable range, $[0.9\Theta_s, 1.1\Theta_s]$. If the total budget exceeds the upper bound, we randomly decrease one or more θ_i . Conversely, if the total budget is below the lower bound, we randomly increase one or more θ_i values until the constraint is met, as shown in Fig. 4.

Generality. Standard EA typically requires generating ground truth videos for multiple sample prompts, which introduces additional computational overhead. In our implementation, we simply select 4 prompts from different genres. While including more prompts could theoretically improve generalization, we observe that it leads to minimal improvement in search outcomes while substantially increasing the search cost. The reason is that different prompts often exhibit a similar robustness trend as shown in Fig. 5. Specifically, for each prompt, we skip one timestep during the denoising process and calculate the MSE loss against the ground truth. By sweeping all the timesteps, we find that different prompts show a similar MSE trend on both OpenSora (Fig. 5a) and Wan (Fig. 5b).

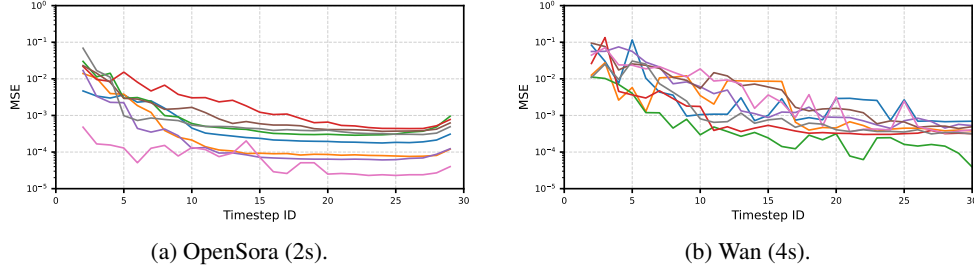


Fig. 5: Different prompts show similar robustness when removing one specific timestep out of the entire denoising process. The MSE is calculated against the original result without skipping timesteps.

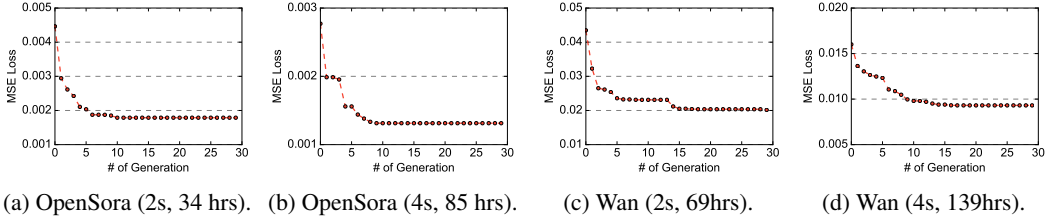


Fig. 6: The MSE loss trend in the EA search process. Here, we only show one case: the performance target is 50% of the token budget reduction. The trend is similar for other cases. The first number in parentheses is the video length, and the second number is the total GPU search hours.

4 Evaluation

4.1 Experimental Setup

Baselines. We evaluate two widely used text-to-video generation frameworks: Wan v2.1 1.3B [29] and OpenSora v1.2 [41]. For each model, we test both short-sequence videos (2-second 480P) and long-sequence videos (4-second 480P). Our evaluation compares with three the state-of-the-art training-free reuse-based methods: Δ -DiT [8], PAB [40], and ToCA [43].

EA Configuration. In our EA algorithm, we set the maximal generation to be 30, each generation selects W to be 50. To ensure diversity of candidates in the early stages and structural stability of good candidates in the later stages, we set P_0 and P_{final} to be 0.1 and 0.01, respectively. Fig. 6 shows the EA search process of one case, 50% of the token budget reduction. Across all four evaluated models, the results converge after searching 30 generations. All EA searches are conducted on 8 A100 GPUs with an average search time of 82 GPU hours.

Metrics and Hardware. Following prior works [40, 43, 33, 8], we use the VBench score [17] as the video quality metric. During the experiments, we generate 5 videos for each of the 950 benchmark prompts using different random seeds. The generated videos are then evaluated across 16 aspects. We report the average value of the aspects. We compare the generated videos by different acceleration methods against the original video results frame-by-frame on image quality, using PSNR, SSIM, and LPIPS. For performance, we report end-to-end generation latency, GPU memory consumption, and computational complexity (FLOPs). Our evaluation uses two GPUs as our hardware platforms: NVidia A6000 with 48 GB of memory and NVidia A100 with 80 GB of memory.

4.2 Performance and Accuracy

Video Quality. Tbl. 1 presents the overall comparison of generation quality across different techniques. On Wan, ASTRAEA achieves the highest speedup (roughly $1.9\times$) while maintaining a better VBench score compared to other baselines. On VBench metric, both $\text{ASTRAEA}_{50\%}$ and $\text{ASTRAEA}_{70\%}$ can retain the accuracy loss within 0.5%. In contrast, the strongest baseline, PAB_{2-6} , achieves only 79.2%, which is 1.0% lower than the original model’s score on Wan (4s). Similarly, on OpenSora, we can achieve almost the best accuracy while achieving the highest speedup. Although Δ -DiT achieves the best VBench score on OpenSora (2s), Δ -DiT can only achieve $1.01\times$ speedup.

Table 1: Quantitative evaluation of our method against the state-of-the-arts [8, 43, 40] on two vDiT models: Wan v2.1 1.3B [29] and OpenSora v1.2 [41]. 🏆 and 🥈 denote the **best** and **second-best** results among all methods, respectively. PAB: The subscript numbers represent the reuse strides for spatial, temporal, and cross-attention. ToCA: The subscript numbers denote the timestep reuse stride and MLP reuse ratio. ASTRAEA: The percentage indicates the total token budget.

Model	Metric Method	Quality Metrics				Performance Metrics					
		VBench (%)↑	PSNR (dB)↑	SSIM↑	LPIPS↓	FLOPs (10 ¹⁵)↓	L _{A100} (sec.)↓	Speedup (A100)	L _{A6000} (sec.)↓	Speedup (A6000)	Mem. (GB)↓
Wan (2s) [29]	Original	81.46	-	-	-	7.29	68.48	1.00	108.30	1.00	7.8
	Δ -DiT [8]	78.37	15.13	0.499	0.408	5.87	60.52	1.13	87.81	1.23	7.81
	PAB _{2_6} [40]	80.05	18.02	0.667	0.246	4.67	50.36	1.36	79.84	1.35	11.59
	PAB _{5_9} [40]	78.61	17.60	0.638	0.290	🥈 3.34	40.31	1.70	66.47	1.62	11.59
	ToCA _{2,80%} [43]	81.06	18.01	0.651	0.254	4.14	44.43	1.54	75.02	1.44	17.66
	ToCA _{2,85%} [43]	80.89	18.02	0.653	0.252	4.07	43.86	1.56	71.28	1.52	17.66
	ASTRAEA 40%	80.82	23.77	0.826	0.144	🏆 3.05	🏆 30.23	🏆 2.27	🏆 46.05	🏆 2.35	9.04
	ASTRAEA 50%	🥈 81.11	🥈 25.67	🥈 0.884	🥈 0.071	3.85	🥈 37.29	🥈 2.01	🥈 56.77	🥈 1.91	9.04
	ASTRAEA 70%	🏆 81.28	🏆 30.83	🏆 0.948	🏆 0.026	5.38	44.71	1.68	77.91	1.39	9.04
Wan (4s) [29]	Original	80.28	-	-	-	19.87	155.01	1.00	253.62	1.00	8.97
	Δ -DiT [8]	76.81	16.14	0.602	0.376	15.96	135.96	1.14	205.17	1.24	8.97
	PAB _{2_6} [40]	78.76	19.95	0.761	0.194	12.79	113.41	1.37	183.37	1.38	15.96
	PAB _{5_9} [40]	77.71	19.44	0.739	0.234	🥈 8.99	90.72	1.71	148.58	1.71	15.96
	ToCA _{2,80%} [43]	79.01	18.10	0.689	0.269	11.04	96.84	1.60	154.83	1.64	38.40
	ToCA _{2,85%} [43]	79.28	18.13	0.694	0.264	10.92	95.07	1.63	152.34	1.66	38.40
	ASTRAEA 40%	79.78	26.98	0.901	0.072	🏆 8.20	🏆 67.61	🏆 2.29	🏆 106.65	🏆 2.38	11.71
	ASTRAEA 50%	🥈 79.96	🥈 28.12	🥈 0.918	🥈 0.053	10.32	🥈 83.34	🥈 1.86	🥈 132.62	🥈 1.91	11.71
	ASTRAEA 70%	🏆 80.18	🏆 33.00	🏆 0.958	🏆 0.021	14.42	114.20	1.36	184.89	1.37	11.71
OpenSora (2s) [41]	Original	78.14	-	-	-	3.29	54.09	1.00	78.10	1.00	14.89
	Δ -DiT [8]	🏆 78.09	29.09	0.906	0.066	2.84	52.83	1.02	77.23	1.01	23.78
	PAB ₂₄₆ [40]	77.50	26.78	0.884	0.089	2.91	44.09	1.23	59.87	1.31	27.20
	PAB ₅₇₉ [40]	75.52	22.60	0.800	0.191	2.53	37.68	1.44	55.75	1.40	27.20
	ToCA _{3,80%} [43]	77.13	20.28	0.766	0.209	1.89	32.04	1.69	53.61	1.45	41.27
	ToCA _{3,85%} [43]	76.89	20.02	0.760	0.216	1.84	31.74	1.70	52.89	1.48	41.27
	ASTRAEA 40%	76.95	27.23	0.875	0.095	🏆 1.50	🏆 22.97	🏆 2.35	🏆 33.67	🏆 2.32	20.08
	ASTRAEA 50%	77.45	🥈 29.52	🥈 0.908	🥈 0.067	🥈 1.82	🥈 28.36	🥈 1.91	🥈 41.13	🥈 1.82	20.08
	ASTRAEA 70%	🥈 78.08	🏆 31.78	🏆 0.932	🏆 0.039	2.48	37.15	1.46	54.54	1.43	20.08
OpenSora (4s) [41]	Original	79.00	-	-	-	6.59	109.15	1.00	173.07	1.00	16.96
	Δ -DiT [8]	🥈 78.46	28.15	0.886	0.084	5.68	108.93	1.00	171.84	1.01	25.83
	PAB ₂₄₆ [40]	78.40	🥈 28.65	🥈 0.896	🥈 0.081	5.82	76.48	1.43	139.52	1.24	41.55
	PAB ₅₇₉ [40]	76.63	23.36	0.804	0.192	5.10	70.71	1.54	129.52	1.34	41.55
	ToCA _{3,80%} [43]	77.69	21.02	0.773	0.212	3.79	65.48	1.67	OOM	OOM	61.17
	ToCA _{3,85%} [43]	77.68	20.72	0.767	0.219	🥈 3.56	64.46	1.69	OOM	OOM	61.17
	ASTRAEA 40%	76.62	25.65	0.841	0.145	🏆 3.00	🏆 47.30	🏆 2.31	🏆 74.63	🏆 2.32	27.98
	ASTRAEA 50%	78.07	28.51	0.891	0.086	3.65	🥈 58.62	🥈 1.86	🥈 92.54	🥈 1.87	27.98
	ASTRAEA 70%	🏆 78.65	🏆 30.92	🏆 0.920	🏆 0.056	4.97	76.13	1.43	121.57	1.42	27.98

In contrast, ASTRAEA 70% is almost the best on all quality metrics with much higher speedup. ASTRAEA 50% can achieve the second or third best on quality metrics while achieving higher speedup with a large margin. In Fig. 7, we show more detailed VBench scores. Across all VBench scores, our variants are closely matched with the original baselines. The qualitative comparison of ASTRAEA against other methods is shown in Fig. 8. Qualitatively, ASTRAEA achieves better consistency with the original models compared to other methods.

Image consistency. In addition to evaluating VBench scores, we also perform frame-to-frame comparisons against the outputs from the original models to assess image consistency. Our results show that ASTRAEA consistently preserves higher image consistency across all evaluated models. In particular, ASTRAEA outperforms all baseline methods by a significant margin on Wan (2s), Wan (4s), and OpenSora (2s) across all image quality metrics. For instance, on both Wan (2s) and Wan (4s), the ASTRAEA 70% outperforms the strongest baseline by 10 dB.

Performance. Tbl. 1 also shows the performance comparison across various models. ASTRAEA consistently outperforms all baselines in both inference speed and GPU memory. For Wan (2s), ASTRAEA 50% can deliver the highest speedup 1.9 \times on both A100 and A6000 with lowest memory usage. Meanwhile, it still delivers the second-best quality against the other methods. On other models, our method also achieves significantly higher speedup. Specifically, when we set the token budget to be 40%, we can achieve 2.4 \times speedup while the model accuracy is still competitive.

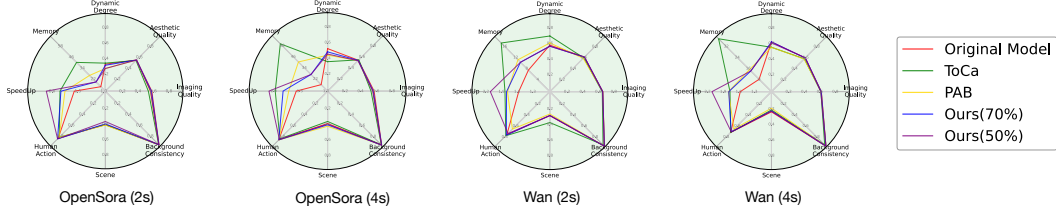


Fig. 7: VBench metrics, speedup, and memory consumption of ASTRAEA against other methods.

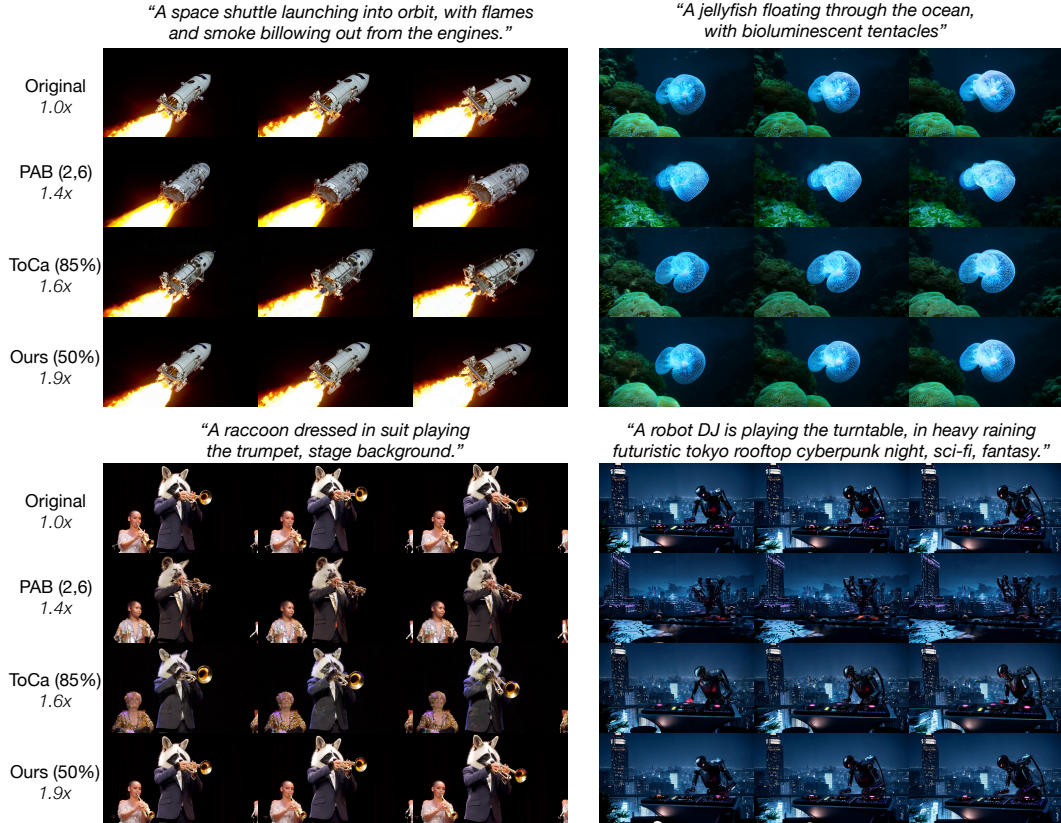


Fig. 8: The qualitative comparison of ASTRAEA against other methods on Wan (4s). The *Italic* numbers show the average speedup against the original baselines.

Scalability. ASTRAEA shows strong performance scalability across various vDiT models. As shown in Fig. 9, our method demonstrates sublinear speedups as the number of GPUs increases across four different models. Specifically, our method can achieve $13.2\times$ speedup on OpenSora with 8 GPUs. Overall, ASTRAEA can achieve over $10\times$ speedup with 8 GPUs. This shows the high parallelizability of our sparse attention mechanism described in Sec. 3.2. Meanwhile, results also indicate that our token selection mechanism has low overhead.

Table 2: The ablation study on Wan (4s).

Method	Quality Metrics				Performance Metrics					
	VBench (%) \uparrow	PSNR (dB) \uparrow	SSIM \uparrow	LPIPS \downarrow	FLOPs (10^{15}) \downarrow	L_{A100} (sec.) \downarrow	Speedup (A100)	L_{A6000} (sec.) \downarrow	Speedup (A6000)	Mem. (GB) \downarrow
Original	80.28	-	-	-	16.54	155.01	-	253.62	-	8.97
<u>TIMSTEP-LEVEL</u>	79.50	22.71	0.802	0.169	10.32	78.51	1.97	127.72	1.99	8.97
<u>FIXED-TOKEN</u>	77.92	19.75	0.753	0.214	10.32	83.20	1.86	132.19	1.91	11.71
<u>ASTRAEA</u>	79.96	28.12	0.918	0.053	10.32	83.34	1.86	132.62	1.91	11.71

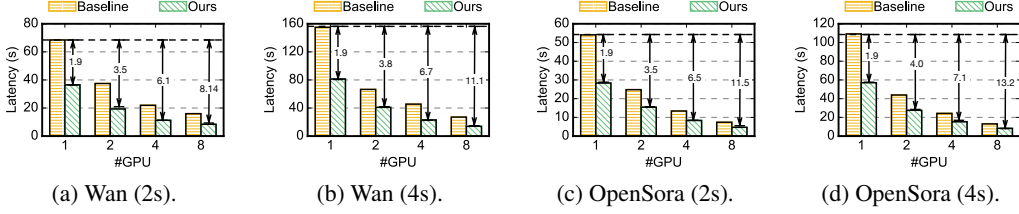


Fig. 9: The speedup of ASTRAEA against the baseline models across various numbers of GPUs.

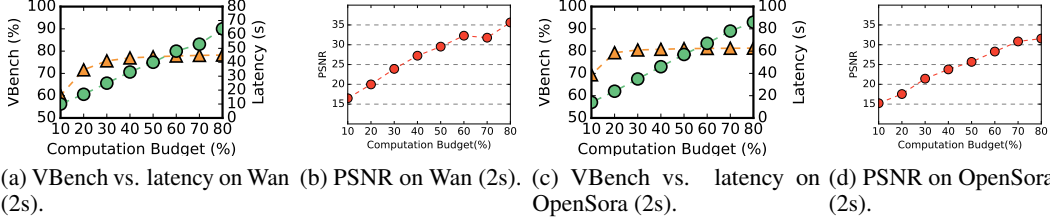


Fig. 10: Sensitivity of computational budget percentage to quality metrics, VBench score and PSNR, and performance on OpenSora (2s) and Wan (2s).

4.3 Ablation Study

In the ablation study, we compare two different granularities: TIMESTEP-LEVEL and FIXED-TOKEN. TIMESTEP-LEVEL only selects timesteps. Each timestep either computes all tokens or skips computation entirely. FIXED-TOKEN selects tokens at the granularity of timesteps instead of blocks. All selected tokens within a timestep are computed, while unselected ones are skipped.

Our experiments show that both TIMESTEP-LEVEL and FIXED-TOKEN achieve much lower VBench scores compared to our method. Specifically, FIXED-TOKEN drops the VBench score significantly ($>2.0\%$). This shows that the important tokens vary across compute blocks. On the other hand, TIMESTEP-LEVEL drops the VBench scores slightly, while achieving a higher speedup compared to our method under the same token budget. This suggests that selecting at the timestep level may be a viable approach when trading off accuracy for higher performance. However, TIMESTEP-LEVEL suffers from noticeably lower image consistency compared to ASTRAEA.

4.4 Sensitivity Study

Fig. 10 shows the sensitivity of the computation budget (expressed as a percentage) to both the overall VBench score and execution latency on Wan (2s) and OpenSora (2s). On both models, we observe that VBench score degrades rapidly when the computation budget drops below around 30%. In contrast, execution latency increases linearly with the computation budget. These results suggest that selecting a computation budget in the range between 30% and 40% offers a favorable trade-off between generation quality and inference efficiency.

5 Conclusion

As vDiTs continue to drive breakthroughs in text-to-video generation, their deployment remains limited by computational demands. This work presents ASTRAEA, a framework that systematically accelerates vDiT inference through fine-grained token-level selection. By combining our three optimizations: a lightweight token selection mechanism, memory-efficient sparse attention, and a hierarchical search framework, ASTRAEA dynamically determines the optimal token allocation at each denoising step. We demonstrate that our method not only delivers significant reductions in inference latency and memory usage but also preserves higher generation quality. Nevertheless, our work still requires a certain search time to find the close-optimal configuration for each model via a stochastic search. A promising direction for future work is to develop a non-stochastic, search-free alternative that can directly infer optimal configurations with even less overhead.

References

- [1] Tencent launches and open-sources Hunyuan video-generation model, 2024.
- [2] Kuaishou Unveils Proprietary Video Generation Model ‘Kling’; Testing Now Available, 2024.
- [3] Sora: Bring your imagination to life with text, image, or video, 2024.
- [4] Veo 2: Our state-of-the-art video generation model, 2024.
- [5] Daniel Ashlock. *Evolutionary computation for modeling and optimization*. Springer, 2006.
- [6] Daniel Bolya and Judy Hoffman. Token merging for fast stable diffusion. In *Proceedings of the IEEE/CVF conference on computer vision and pattern recognition*, pages 4599–4603, 2023.
- [7] Daniel Bolya, Cheng-Yang Fu, Xiaoliang Dai, Peizhao Zhang, Christoph Feichtenhofer, and Judy Hoffman. Token merging: Your vit but faster. *arXiv preprint arXiv:2210.09461*, 2022.
- [8] Pengtao Chen, Mingzhu Shen, Peng Ye, Jianjian Cao, Chongjun Tu, Christos-Savvas Bouganis, Yiren Zhao, and Tao Chen. Delta-dit: A training-free acceleration method tailored for diffusion transformers. *arXiv preprint arXiv:2406.01125*, 2024.
- [9] Hongrong Cheng, Miao Zhang, and Javen Qinfeng Shi. A survey on deep neural network pruning: Taxonomy, comparison, analysis, and recommendations. *IEEE Transactions on Pattern Analysis and Machine Intelligence*, 2024.
- [10] Tri Dao. Flashattention-2: Faster attention with better parallelism and work partitioning. *arXiv preprint arXiv:2307.08691*, 2023.
- [11] Tri Dao, Dan Fu, Stefano Ermon, Atri Rudra, and Christopher Ré. Flashattention: Fast and memory-efficient exact attention with io-awareness. *Advances in Neural Information Processing Systems*, 35: 16344–16359, 2022.
- [12] Thomas Elsken, Jan Hendrik Metzen, and Frank Hutter. Neural architecture search: A survey. *Journal of Machine Learning Research*, 20(55):1–21, 2019.
- [13] Gongfan Fang, Xinyin Ma, and Xinchao Wang. Structural pruning for diffusion models. In *Advances in Neural Information Processing Systems*, 2023.
- [14] Jiatao Gu, Shuangfei Zhai, Yizhe Zhang, Lingjie Liu, and Joshua M Susskind. Boot: Data-free distillation of denoising diffusion models with bootstrapping. In *ICML 2023 Workshop on Structured Probabilistic Inference & Generative Modeling*, 2023.
- [15] Amirhossein Habibian, Amir Ghodrati, Noor Fathima, Guillaume Sautiere, Risheek Garrepalli, Fatih Porikli, and Jens Petersen. Clockwork diffusion: Efficient generation with model-step distillation. In *Proceedings of the IEEE/CVF Conference on Computer Vision and Pattern Recognition*, pages 8352–8361, 2024.
- [16] Torsten Hoefer, Dan Alistarh, Tal Ben-Nun, Nikoli Dryden, and Alexandra Peste. Sparsity in deep learning: Pruning and growth for efficient inference and training in neural networks. *Journal of Machine Learning Research*, 22(241):1–124, 2021.
- [17] Ziqi Huang, Yanan He, Jiashuo Yu, Fan Zhang, Chenyang Si, Yuming Jiang, Yuanhan Zhang, Tianxing Wu, Qingyang Jin, Nattapol Chanpaisit, et al. Vbench: Comprehensive benchmark suite for video generative models. In *Proceedings of the IEEE/CVF Conference on Computer Vision and Pattern Recognition*, pages 21807–21818, 2024.
- [18] Kumara Kahatapitiya, Haozhe Liu, Sen He, Ding Liu, Menglin Jia, Michael S Ryoo, and Tian Xie. Adaptive caching for faster video generation with diffusion transformers. *arXiv preprint arXiv:2411.02397*, 2024.
- [19] Bo-Kyeong Kim, Hyoung-Kyu Song, Thibault Castells, and Shinkook Choi. Bk-sdm: A lightweight, fast, and cheap version of stable diffusion. In *European Conference on Computer Vision*, pages 381–399. Springer, 2024.
- [20] Weijie Kong, Qi Tian, Zijian Zhang, Rox Min, Zuozhuo Dai, Jin Zhou, Jiangfeng Xiong, Xin Li, Bo Wu, Jianwei Zhang, et al. Hunyuanvideo: A systematic framework for large video generative models. *arXiv preprint arXiv:2412.03603*, 2024.

- [21] Lijiang Li, Huixia Li, Xiawu Zheng, Jie Wu, Xuefeng Xiao, Rui Wang, Min Zheng, Xin Pan, Fei Chao, and Rongrong Ji. Autodiffusion: Training-free optimization of time steps and architectures for automated diffusion model acceleration. In *Proceedings of the IEEE/CVF International Conference on Computer Vision*, pages 7105–7114, 2023.
- [22] Bin Lin, Yunyang Ge, Xinhua Cheng, Zongjian Li, Bin Zhu, Shaodong Wang, Xianyi He, Yang Ye, Shenghai Yuan, Liuhan Chen, et al. Open-sora plan: Open-source large video generation model. *arXiv preprint arXiv:2412.00131*, 2024.
- [23] Feng Liu, Shiwei Zhang, Xiaofeng Wang, Yujie Wei, Haonan Qiu, Yuzhong Zhao, Yingya Zhang, Qixiang Ye, and Fang Wan. Timestep embedding tells: It’s time to cache for video diffusion model. *arXiv preprint arXiv:2411.19108*, 2024.
- [24] Joseph Liu, Joshua Geddes, Ziyu Guo, Haomiao Jiang, and Mahesh Kumar Nandwana. Smoothcache: A universal inference acceleration technique for diffusion transformers. *arXiv preprint arXiv:2411.10510*, 2024.
- [25] Zhengyao Lv, Chenyang Si, Junhao Song, Zhenyu Yang, Yu Qiao, Ziwei Liu, and Kwan-Yee K Wong. Fastercache: Training-free video diffusion model acceleration with high quality. *arXiv preprint arXiv:2410.19355*, 2024.
- [26] Xinyin Ma, Gongfan Fang, and Xinchao Wang. Deepcache: Accelerating diffusion models for free. In *Proceedings of the IEEE/CVF Conference on Computer Vision and Pattern Recognition*, pages 15762–15772, 2024.
- [27] Junxiang Qiu, Lin Liu, Shuo Wang, Jinda Lu, Kezhou Chen, and Yanbin Hao. Accelerating diffusion transformer via gradient-optimized cache. *arXiv preprint arXiv:2503.05156*, 2025.
- [28] Tim Salimans and Jonathan Ho. Progressive distillation for fast sampling of diffusion models. *arXiv preprint arXiv:2202.00512*, 2022.
- [29] Ang Wang, Baole Ai, Bin Wen, Chaojie Mao, Chen-Wei Xie, Di Chen, Fei Wu Yu, Haiming Zhao, Jianxiao Yang, Jianyuan Zeng, Jiayu Wang, Jingfeng Zhang, Jingren Zhou, Jinkai Wang, Jixuan Chen, Kai Zhu, Kang Zhao, Keyu Yan, Lianghua Huang, Mengyang Feng, Ningyi Zhang, Pandeng Li, Pingyu Wu, Ruihang Chu, Ruili Feng, Shiwei Zhang, Siyang Sun, Tao Fang, Tianxing Wang, Tianyi Gui, Tingyu Weng, Tong Shen, Wei Lin, Wei Wang, Wei Wang, Wenmeng Zhou, Wenten Wang, Wenting Shen, Wenyuan Yu, Xianzhong Shi, Xiaoming Huang, Xin Xu, Yan Kou, Yangyu Lv, Yifei Li, Yijing Liu, Yiming Wang, Yingya Zhang, Yitong Huang, Yong Li, You Wu, Yu Liu, Yulin Pan, Yun Zheng, Yuntao Hong, Yupeng Shi, Yutong Feng, Zeyinzi Jiang, Zhen Han, Zhi-Fan Wu, and Ziyu Liu. Wan: Open and advanced large-scale video generative models. *arXiv preprint arXiv:2503.20314*, 2025.
- [30] Colin White, Mahmoud Safari, Rhea Sukthanker, Binxin Ru, Thomas Elsken, Arber Zela, Debadeepta Dey, and Frank Hutter. Neural architecture search: Insights from 1000 papers. *arXiv preprint arXiv:2301.08727*, 2023.
- [31] Darrell Whitley, Soraya Rana, John Dzubera, and Keith E Mathias. Evaluating evolutionary algorithms. *Artificial intelligence*, 85(1-2):245–276, 1996.
- [32] Felix Wimbauer, Bichen Wu, Edgar Schoenfeld, Xiaoliang Dai, Ji Hou, Zijian He, Artsiom Sanakoyeu, Peizhao Zhang, Sam Tsai, Jonas Kohler, et al. Cache me if you can: Accelerating diffusion models through block caching. In *Proceedings of the IEEE/CVF Conference on Computer Vision and Pattern Recognition*, pages 6211–6220, 2024.
- [33] Haocheng Xi, Shuo Yang, Yilong Zhao, Chenfeng Xu, Muyang Li, Xiuyu Li, Yujun Lin, Han Cai, Jintao Zhang, Dacheng Li, et al. Sparse videogen: Accelerating video diffusion transformers with spatial-temporal sparsity. *arXiv preprint arXiv:2502.01776*, 2025.
- [34] Ling Yang, Zhilong Zhang, Yang Song, Shenda Hong, Runsheng Xu, Yue Zhao, Yingxia Shao, Wentao Zhang, Bin Cui, and Ming-Hsuan Yang. Diffusion models: A comprehensive survey of methods and applications. *arxiv* 2022. *arXiv preprint arXiv:2209.00796*, 2022.
- [35] Tianwei Yin, Michaël Gharbi, Richard Zhang, Eli Shechtman, Fredo Durand, William T Freeman, and Taesung Park. One-step diffusion with distribution matching distillation. In *Proceedings of the IEEE/CVF Conference on Computer Vision and Pattern Recognition*, pages 6613–6623, 2024.
- [36] Hui Zhang, Zuxuan Wu, Zhen Xing, Jie Shao, and Yu-Gang Jiang. Adadiff: Adaptive step selection for fast diffusion. *arXiv preprint arXiv:2311.14768*, 2023.

- [37] Hui Zhang, Tingwei Gao, Jie Shao, and Zuxuan Wu. Blockdance: Reuse structurally similar spatio-temporal features to accelerate diffusion transformers. *arXiv preprint arXiv:2503.15927*, 2025.
- [38] Hanling Zhang, Rundong Su, Zhihang Yuan, Pengtao Chen, Mingzhu Shen Yibo Fan, Shengen Yan, Guohao Dai, and Yu Wang. Ditfastattnv2: Head-wise attention compression for multi-modality diffusion transformers. *arXiv preprint arXiv:2503.22796*, 2025.
- [39] Peiyuan Zhang, Yongqi Chen, Runlong Su, Hangliang Ding, Ion Stoica, Zhenghong Liu, and Hao Zhang. Fast video generation with sliding tile attention. *arXiv preprint arXiv:2502.04507*, 2025.
- [40] Xuanlei Zhao, Xiaolong Jin, Kai Wang, and Yang You. Real-time video generation with pyramid attention broadcast. *arXiv preprint arXiv:2408.12588*, 2024.
- [41] Zangwei Zheng, Xiangyu Peng, Tianji Yang, Chenhui Shen, Shenggui Li, Hongxin Liu, Yukun Zhou, Tianyi Li, and Yang You. Open-sora: Democratizing efficient video production for all, 2024.
- [42] Chang Zou, Xuyang Liu, Ting Liu, Siteng Huang, and Linfeng Zhang. Toca: Accelerating diffusion transformers with token-wise feature caching. <https://github.com/Shenyi-Z/ToCa>, 2024.
- [43] Chang Zou, Xuyang Liu, Ting Liu, Siteng Huang, and Linfeng Zhang. Accelerating diffusion transformers with token-wise feature caching. *arXiv preprint arXiv:2410.05317*, 2024.

A Supplementary

A.1 Algorithm

A.1.1 Token Selection Algorithm

Algo. 1 illustrates our lightweight token selection mechanism detailed in Sec. 3.2. Overall, our algorithm dynamically selects tokens required for computation based on their significance and imposes a penalty for consecutive non-selection.

Algorithm 1 Efficient Attention via Temporal Token Selection.

Require: $X_{t-1}, X_t \in \mathbb{R}^{N \times D}$	▷ Token features at timestep $t-1$ and t
Require: k	▷ Number of tokens to attend (top- k)
Require: W_Q, W_K, W_V	▷ Projection matrices
Ensure: $X'_t \in \mathbb{R}^{N \times D}$	▷ Updated token features at t
1: $\Delta_t \leftarrow \text{Mean}((X_t - X_{t-1}), \text{dim} = 1) \cdot S_{\text{LSE}_{t-1}}$	▷ Per-token squared difference
2: $S_t \leftarrow \text{TopK}(\Delta_t, k)$	▷ Selected token indices (top- k)
3: $Q \leftarrow X_t W_Q, K \leftarrow X_t W_K, V \leftarrow X_t W_V$	▷ Project all tokens
4: $Q_{\text{sel}} \leftarrow Q[S_t]$	▷ Select Query vectors for top- k tokens
5: $\hat{X}[S_t] \leftarrow \text{Softmax}(Q_{\text{sel}} K^\top / \sqrt{d}) V$	▷ Compute attention only for selected Query
6: $\hat{X}[\text{others}] \leftarrow X_t[\text{others}]$	▷ Unselected tokens remain unchanged or reused
7: return \hat{X}	

A.1.2 Token-Wise Search Algorithm

Algo. 2 outlines our token-wise search algorithm via an evolutionary algorithm. This algorithm is used to determine the optimal token budget allocation across denoising timesteps, as discussed in Sec. 3.3. The overall logic of this algorithm iteratively refines candidates through crossover, mutation, and repair operations to achieve a target performance with minimal accuracy loss.

A.2 Experimental Setup

Hardware Platforms. We conduct both the performance and accuracy measurements on two hardware platforms:

- NVIDIA A6000 with 38.71 TFLOPS (FP32) and 48 GB memory;
- NVIDIA A100 with 19.49 TFLOPS (FP32) and 80 GB memory.

Video Generation Frameworks. We measure the performance of various acceleration techniques on two widely-used video generation frameworks: Wan v2.1 1.3 B [29] and OpenSora v1.2 [41]. We test both models on 2-second videos and 4-second videos with 480p resolution.

Baselines. We compare against three different training-free acceleration techniques:

- Δ -DiT [8]. The parameter b represents the timestep at which the reusing strategy of the block residuals switches. The parameter N represents the timestep intervals that skip full computation. In OpenSora, we set b and N to be 15 and 3, respectively. The partial computation starts at timestep 3 and ends at timestep 28. We also preserve the residuals of the first 10 blocks or the last 10 blocks. In Wan model, we set b and N to be 25 and 3, respectively. The partial computation starts at timestep 5 and ends at timestep 45. We also preserve the residuals of the first 10 blocks or the last 10 blocks.
- PAB [40]. The broadcast range n represents the timestep intervals that skip full computation. In the OpenSora model, the broadcast ranges of spatial attention, temporal attention, and cross-attention are set to be (2, 4, 6) or (5, 7, 9). Similarly, in the Wan model, the broadcast ranges of self-attention and cross-attention are set to be (2, 6) or (5, 9). Meanwhile, for both models, we keep the first 15% and last 15% of the timesteps untouched.

Algorithm 2 Evolutionary Search for Token Scheduling.

Require: T ▷ Total timesteps (e.g., 100)
Require: B ▷ Computation budget (e.g., total cost ≤ 50)
Require: P ▷ Prompt set for evaluation
Require: N ▷ Population size
Require: G ▷ Number of generations
Ensure: Best scheduling sequence $\mathbf{r}^* = [r_1, r_2, \dots, r_T]$
1: Initialize population $\mathcal{S} = \{\mathbf{r}^{(1)}, \dots, \mathbf{r}^{(N)}\}$ with $\sum_{t=1}^T r_t \leq B$
2: **for** $g = 1$ to G **do**
3: **for all** $\mathbf{r}^{(i)} \in \mathcal{S}$ **do**
4: Compute fitness: $\text{MSE}^{(i)} \leftarrow \text{Evaluate}(\mathbf{r}^{(i)}, P)$
5: **end for**
6: Select top individuals as parents: $\mathcal{P} \subset \mathcal{S}$
7: Initialize new population: $\mathcal{S}_{\text{new}} \leftarrow \emptyset$
8: **while** $|\mathcal{S}_{\text{new}}| < N$ **do**
9: Sample parents $\mathbf{r}^{(a)}, \mathbf{r}^{(b)} \in \mathcal{P}$
10: $\mathbf{r}_{\text{child}} \leftarrow \text{Crossover}(\mathbf{r}^{(a)}, \mathbf{r}^{(b)})$
11: $\mathbf{r}_{\text{child}} \leftarrow \text{Mutate}(\mathbf{r}_{\text{child}})$
12: $\mathbf{r}_{\text{child}} \leftarrow \text{RepairIfNeeded}(\mathbf{r}_{\text{child}}, B)$
13: **if** $\mathbf{r}_{\text{child}} \notin \mathcal{S}_{\text{new}}$ **then**
14: Add $\mathbf{r}_{\text{child}}$ to \mathcal{S}_{new}
15: **end if**
16: **end while**
17: $\mathcal{S} \leftarrow \mathcal{S}_{\text{new}}$
18: **end for**
19: **return** $\arg \min_{\mathbf{r} \in \mathcal{S}} \text{MSE}(\mathbf{r}, P)$

- **TOCA** [43]: This variant is similar to **PAB**. However, **TOCA** also performs a certain level of token-wise skipping similar to our work. We faithfully reimplement their work according to their released code [42], which only applies the token selection on cross-attention and MLP layers. In OpenSora, their broadcast ranges of spatial attention, temporal attention, cross-attention, and MLP are 3, 3, 6, and 3, respectively. The reuse ratios of MLP in their two variants are set to 80% and 85%, respectively. In Wan model, their broadcast ranges of spatial attention, temporal attention, cross-attention, and MLP are 2, 2, 2, and 2, respectively. The reuse ratios of MLP in their two variants are also set to 80% and 85%, respectively.

Evaluation Metrics. Next, we describe how we obtain various performance and quality metrics.

- **Video Quality.** We used the VBench score [17] as the primary video quality metric. For each of the 946 benchmark prompts, 5 videos were generated using different random seeds. The generated videos are then evaluated across 16 aspects. We then report the average value of the aspects. The VBench score is obtained from the VBENCH benchmark suite [17]. Specific APIs within this suite are used to evaluate aspects like Motion Fidelity, Temporal Consistency, Aesthetic Quality, etc.
- **Image Consistency (PSNR, SSIM, LPIPS).** To assess frame-to-frame image consistency, we compared generated videos by different acceleration methods against the original video results on image quality, using PSNR, SSIM, and LPIPS. PSNR is calculated using standard image processing libraries, e.g., `skimage.metrics.peak_signal_noise_ratio`. Similarly, SSIM is calculated using `skimage.metrics.structural_similarity`. LPIPS is measured using a the `lpips` library in Python.
- **Performance.** For performance, we report end-to-end generation latency, GPU memory consumption, and computational complexity (FLOPs). For end-to-end latency, we measure the total time elapsed during video generation. Here, we use Python’s `torch.cuda` module. We capture the start and end timestamps using `torch.cuda.event()` and use the difference between these two as the end-to-end latency. For GPU memory consumption, we use the built-in measurement to monitor the peak GPU memory usage during inference. For FLOPs, we design an analytic model to calculate the floating-point operations. Please see Sec. A.3.

A.3 FLOPs Calculation Formulations

Input Representation. We first define the symbols we used in our FLOPs computation:

- B : Batch size.
- N : Number of tokens (sequence length).
- H : Embedding dimension (hidden dimension).
- N_{head} : Number of attention heads.
- $d = H/N_{\text{head}}$: Dimension per head.

A.3.1 Attention FLOPs Calculation

We abstract the computation of an attention module into two parts: linear projections for Query (Q), Key (K), and Value (V), and the subsequent attention score computations.

Linear Projection. The input $X \in \mathbb{R}^{B \times N \times H}$ is projected into Q , K , and V tensors, each of shape $\mathbb{R}^{B \times N \times H}$. A single linear transformation of shape $[H \times H]$ has a FLOPs count of $2 \times B \times N \times H \times H$. Therefore, the total FLOPs for Q , K , and V projections can be expressed as,

$$f_{qkv} = 3 \times (2 \times B \times N \times H \times H) = 6BNH^2. \quad (9)$$

Attention Score Computation. This step includes calculating the attention scores, applying softmax, computing the attention output, and output linear projection. We next describe these four parts separately.

1. **Compute Attention Scores (QK^T).** Initially, the input shapes of Q and K are both $[B, N_{\text{head}}, N, d]$. Their product, QK^T , results in a tensor of shape $[B, N_{\text{head}}, N, N]$. The FLOPs for computing QK^T per head are $2 \times N \times d \times N$. If we sum across all heads and batches, the total FLOPs becomes: $FLOPs_{QK^T} = 2 \times B \times N_{\text{head}} \times N \times d \times N = 2BN_{\text{head}}N^2d$.
2. **Softmax Operation.** The softmax operation is applied to the QK^T scores. Its computational cost is relatively small compared to matrix multiplications and can be approximated as: $FLOPs_{\text{softmax}} \approx B \times N_{\text{head}} \times N \times N$. For overall computational complexity, its contribution is often considered negligible.
3. **Attention Output ($A \cdot V$).** There are two inputs in this step: the attention map, A , which has a shape of $[B, N_{\text{head}}, N, N]$; and the value, V , with a shape of $[B, N_{\text{head}}, N, d]$. The attention output has a shape of $[B, N_{\text{head}}, N, d]$. The FLOPs to compute $A \cdot V$ is expressed as, $FLOPs_{AV} = 2 \times B \times N_{\text{head}} \times N^2 \times d$.
4. **Output Linear Projection (Head Merging).** Finally, the outputs from all heads are concatenated and passed through a linear layer of shape $[H \times H]$ to produce the final attention output. $FLOPs_{\text{proj}} = 2 \times B \times N \times H^2$.

Total Self-Attention FLOPs. By substituting $d = H/N_{\text{head}}$ and combining the above calculations, the total FLOPs for a self-attention layer simplify to,

$$FLOPs_{\text{attn-total}} = 8BNH^2 + 4BN^2H. \quad (10)$$

A.3.2 Cross-Attention FLOPs Calculation

Cross-attention is similar to self-attention, but its Q and K often come from different input tokens. Here, we define N_q be the number of query tokens and N_{kv} be the number of key/value tokens. The FLOPs calculation can be expressed as, $FLOPs_{\text{cross-attn}} = 4BN_qH^2 + 4BN_{kv}H^2 + 4BN_qN_{kv}H$.

A.3.3 MLP FLOPs Calculation

The MLP in a Transformer typically consists of two linear layers separated by an activation function (e.g., GELU). Here, we ignore the computation of the activation function and only consider the FLOPs in two linear layers. The total FLOPs for an MLP block are, $FLOPs_{\text{mlp}} = 8BNH^2 + 8BNH^2 = 16BNH^2$.

A.4 Full Performance Metrics

In the remaining section, we show the detailed experimental results.

Table 3: Individual VBench scores for OpenSora (4s) model.

Metric	Original	ASTRAEA 70%	ASTRAEA 50%	ASTRAEA 40%	ToCa 80%	ToCa 85%	PAB ₂₄₆	PAB ₅₇₉	Δ -DiT
Subject Consistency	0.9478	0.9471	0.9459	0.9340	0.9475	0.9462	0.9482	0.9360	0.9504
Motion Smoothness	0.9851	0.9872	0.9865	0.9751	0.9844	0.9842	0.9885	0.9889	0.9817
Dynamic Degree	0.5417	0.5000	0.4722	0.4861	0.3750	0.3750	0.4583	0.4028	0.4028
Aesthetic Quality	0.5560	0.5533	0.5483	0.5315	0.5637	0.5633	0.5509	0.5322	0.5601
Imaging Quality	0.5932	0.5831	0.5750	0.5498	0.5535	0.5537	0.5783	0.5509	0.5974
Overall Consistency	0.2742	0.2734	0.2718	0.2656	0.2716	0.2720	0.2734	0.2611	0.2635
Background Consistency	0.9751	0.9745	0.9718	0.9699	0.9695	0.9700	0.9713	0.9637	0.9767
Object Class	0.8062	0.8014	0.7903	0.8030	0.8687	0.8552	0.7967	0.7856	0.8972
Multiple Objects	0.4977	0.4947	0.4703	0.4566	0.5213	0.5358	0.5137	0.4764	0.5793
Color	0.7925	0.8047	0.8221	0.7814	0.8806	0.8659	0.8203	0.7871	0.8179
Spatial Relationship	0.6326	0.6149	0.6036	0.5724	0.6168	0.6308	0.6035	0.5979	0.5705
Scene	0.4135	0.4302	0.4215	0.4208	0.3874	0.3917	0.4484	0.3953	0.4564
Temporal Style	0.2412	0.2406	0.2390	0.2351	0.2481	0.2481	0.2393	0.2319	0.2384
Human Action	0.8800	0.8800	0.8700	0.8600	0.8600	0.8500	0.8800	0.8400	0.8900
Temporal Flickering	0.9952	0.9951	0.9946	0.9922	0.9946	0.9947	0.9951	0.9946	0.9937
Appearance Style	0.2380	0.2379	0.2374	0.2357	0.2381	0.2394	0.2377	0.2357	0.2361
Quality Score	0.8107	0.8064	0.8009	0.7859	0.7911	0.7909	0.8023	0.7871	0.7997
Semantic Score	0.7068	0.7071	0.7003	0.6873	0.7200	0.7202	0.7111	0.6830	0.7239
Total Score	0.7899	0.7865	0.7807	0.7662	0.7769	0.7768	0.7840	0.7663	0.7846

Table 4: Individual VBench scores for OpenSora (2s) model.

Metric	Original	ASTRAEA 70%	ASTRAEA 50%	ASTRAEA 40%	ToCa 80%	ToCa 85%	PAB ₂₄₆	PAB ₅₇₉	Δ -DiT
Subject Consistency	0.9664	0.9675	0.9682	0.9615	0.9576	0.9570	0.9662	0.9591	0.9615
Motion Smoothness	0.9845	0.9864	0.9878	0.9826	0.9854	0.9853	0.9875	0.9885	0.9802
Dynamic Degree	0.3333	0.2917	0.3056	0.3611	0.3194	0.2917	0.2500	0.4286	0.4444
Aesthetic Quality	0.5681	0.5684	0.5676	0.5582	0.5592	0.5584	0.5683	0.5398	0.5463
Imaging Quality	0.5992	0.5930	0.5827	0.5771	0.5545	0.5554	0.5798	0.5376	0.5550
Overall Consistency	0.2722	0.2721	0.2701	0.2698	0.2723	0.2724	0.2709	0.2624	0.2469
Background Consistency	0.9790	0.9781	0.9734	0.9753	0.9717	0.9691	0.9766	0.9630	0.9738
Object Class	0.8347	0.8402	0.8402	0.8354	0.8473	0.8544	0.8576	0.8331	0.9531
Multiple Objects	0.4177	0.4238	0.4040	0.4070	0.4451	0.4261	0.4200	0.3636	0.6602
Color	0.7947	0.8013	0.7762	0.7693	0.7373	0.7539	0.7383	0.7995	0.7538
Spatial Relationship	0.5854	0.5779	0.5702	0.5673	0.5225	0.5381	0.5793	0.5231	0.4717
Scene	0.4295	0.4215	0.3910	0.3903	0.4331	0.4331	0.4368	0.3474	0.5441
Temporal Style	0.2470	0.2466	0.2449	0.2442	0.2455	0.2455	0.2435	0.2351	0.2389
Human Action	0.8600	0.8700	0.8700	0.8600	0.8400	0.8500	0.8400	0.8300	0.9000
Temporal Flickering	0.9947	0.9946	0.9947	0.9932	0.9942	0.9943	0.9946	0.9940	0.9931
Appearance Style	0.2407	0.2402	0.2397	0.2385	0.2420	0.2423	0.2403	0.2384	0.2406
Quality Score	0.8022	0.8012	0.7962	0.7908	0.7922	0.7883	0.7960	0.7780	0.7934
Semantic Score	0.6982	0.6991	0.6878	0.6845	0.6876	0.6912	0.6912	0.6637	0.7308
Total Score	0.7814	0.7808	0.7745	0.7695	0.7713	0.7689	0.7750	0.7552	0.7809

Table 5: Individual VBench scores for Wan (4s) model.

Metric	Original	ASTRAEA 70%	ASTRAEA 50%	ASTRAEA 40%	ToCa 80%	ToCa 85%	PAB ₂₆	PAB ₅₀	Δ -DiT
Subject Consistency	0.9576	0.9579	0.9585	0.9591	0.9478	0.9480	0.9556	0.9557	0.9510
Motion Smoothness	0.9826	0.9828	0.9830	0.9832	0.9816	0.9821	0.9831	0.9839	0.9802
Dynamic Degree	0.6389	0.6389	0.6250	0.6111	0.5694	0.5833	0.5694	0.5139	0.5714
Aesthetic Quality	0.6116	0.6123	0.6162	0.6169	0.5966	0.6004	0.5921	0.5837	0.5566
Imaging Quality	0.6410	0.6392	0.6331	0.6316	0.6348	0.6363	0.6387	0.6214	0.5730
Overall Consistency	0.2361	0.2362	0.2355	0.2343	0.2396	0.2387	0.2248	0.2191	0.2291
Background Consistency	0.9888	0.9888	0.9892	0.9894	0.9668	0.9683	0.9901	0.9901	0.9798
Object Class	0.7587	0.7658	0.7619	0.7611	0.7682	0.7682	0.7650	0.7350	0.7969
Multiple Objects	0.5663	0.5518	0.5450	0.5396	0.5450	0.5587	0.4482	0.4002	0.3516
Color	0.8754	0.8751	0.8715	0.8895	0.8990	0.9079	0.8709	0.8786	0.8438
Spatial Relationship	0.7286	0.7224	0.7001	0.6841	0.7717	0.7846	0.6608	0.6171	0.7447
Scene	0.2594	0.2485	0.2485	0.2238	0.2347	0.2166	0.2122	0.2064	0.1066
Temporal Style	0.2416	0.2408	0.2394	0.2384	0.2451	0.2445	0.2269	0.2172	0.2403
Human Action	0.7400	0.7300	0.7300	0.7300	0.7400	0.7500	0.6800	0.6700	0.6500
Temporal Flickering	0.9943	0.9938	0.9929	0.9924	0.9903	0.9910	0.9941	0.9929	0.9898
Appearance Style	0.1992	0.1988	0.1987	0.1982	0.1995	0.1991	0.1979	0.1986	0.2046
Quality Score	0.8370	0.8368	0.8353	0.8342	0.8199	0.8227	0.8284	0.8202	0.8067
Semantic Score	0.6660	0.6614	0.6567	0.6521	0.6710	0.6730	0.6240	0.6050	0.6135
Total Score	0.8028	0.8018	0.7996	0.7978	0.7901	0.7928	0.7876	0.7771	0.7681

Table 6: Individual VBench scores for Wan (2s) model.

Metric	Original	ASTRAEA 70%	ASTRAEA 50%	ASTRAEA 40%	ToCa 80%	ToCa 85%	PAB ₂₆	PAB ₅₀	Δ -DiT
Subject Consistency	0.9719	0.9722	0.9719	0.9726	0.9575	0.9506	0.9705	0.9684	0.9605
Motion Smoothness	0.9833	0.9832	0.9832	0.9816	0.9811	0.9819	0.9835	0.9836	0.9779
Dynamic Degree	0.5972	0.5833	0.5833	0.5833	0.7143	0.6389	0.6250	0.6250	0.5417
Aesthetic Quality	0.6279	0.6272	0.6278	0.6351	0.6142	0.6208	0.6057	0.5882	0.5906
Imaging Quality	0.6801	0.6788	0.6773	0.6642	0.6723	0.6717	0.6793	0.6630	0.6463
Overall Consistency	0.2383	0.2378	0.2386	0.2370	0.2175	0.2409	0.2266	0.2198	0.2335
Background Consistency	0.9884	0.9889	0.9887	0.9897	0.9656	0.9662	0.9885	0.9884	0.9789
Object Class	0.7595	0.7634	0.7832	0.7627	0.8906	0.8022	0.7381	0.6843	0.7191
Multiple Objects	0.6654	0.6700	0.6441	0.6159	0.4492	0.6601	0.4192	0.3377	0.4710
Color	0.9188	0.8857	0.8714	0.9350	0.8978	0.8705	0.8662	0.8431	0.8227
Spatial Relationship	0.7988	0.8023	0.7888	0.7441	0.7573	0.8283	0.7446	0.6400	0.7368
Scene	0.3089	0.3045	0.3067	0.2907	0.3971	0.3743	0.2871	0.2536	0.2304
Temporal Style	0.2345	0.2337	0.2328	0.2309	0.2285	0.2322	0.2175	0.2061	0.2202
Human Action	0.7800	0.7900	0.7600	0.7900	0.8000	0.7500	0.6800	0.5900	0.7200
Temporal Flickering	0.9900	0.9893	0.9887	0.9853	0.9848	0.9862	0.9907	0.9891	0.9876
Appearance Style	0.1994	0.1985	0.1981	0.1986	0.1962	0.2005	0.1951	0.1956	0.2049
Quality Score	0.8434	0.8418	0.8414	0.8385	0.8385	0.8335	0.8422	0.8360	0.8203
Semantic Score	0.6994	0.6968	0.6898	0.6868	0.6991	0.7105	0.6338	0.5867	0.6371
Total Score	0.8146	0.8128	0.8111	0.8082	0.8106	0.8089	0.8005	0.7861	0.7837

Table 7: FLOPs Breakdown for OpenSora (2s) model across different methods (in 10^{15} FLOPs).

Method	Spatial	Temporal	Cross	MLP
Original	0.7190	0.4282	0.4380	0.8508
Delta-DiT	0.5512	0.3283	0.3358	0.6523
ToCa 0.8	0.2876	0.1713	0.3504	0.4424
ToCa 0.85	0.2450	0.1287	0.1802	0.4169
PAB 246	0.4673	0.2034	0.1825	0.8508
PAB 579	0.3163	0.1713	0.1654	0.8508
Ours 0.5	0.3595	0.2141	0.2190	0.4254
Ours 0.7	0.5033	0.2997	0.3066	0.5956
Ours 0.4	0.2876	0.1713	0.1752	0.3403

Table 8: FLOPs Breakdown for OpenSora (4s) model across different methods (in 10^{15} FLOPs).

Method	Spatial	Temporal	Cross	MLP
Original	1.4379	0.8619	0.8759	1.7016
Delta-DiT	1.1024	0.6608	0.6715	1.3046
ToCa 0.8	0.5752	0.3447	0.7007	0.8848
ToCa 0.85	0.2450	0.1287	0.1802	0.8338
PAB 246	0.9347	0.4094	0.3650	1.7016
PAB 579	0.6327	0.3447	0.3309	1.7016
Ours 0.5	0.7190	0.4309	0.4380	0.8508
Ours 0.7	1.0065	0.6033	0.6131	1.1911
Ours 0.4	0.5752	0.3447	0.3504	0.6806

Table 9: FLOPs Breakdown for Wan (2s) model across different methods (in 10^{15} FLOPs).

Method	Spatial	Cross	MLP
Original	3.6830	0.1491	1.5900
Delta-DiT	2.9464	0.1192	1.2720
ToCa 0.8	1.9520	0.0790	0.9921
ToCa 0.85	1.9520	0.0790	0.9548
PAB 246	2.3940	0.0621	1.5900
PAB 579	1.6205	0.0563	1.5900
Ours 0.5	1.8415	0.0745	0.7950
Ours 0.7	2.5781	0.1043	1.1130
Ours 0.4	1.4732	0.0596	0.6360

Table 10: FLOPs Breakdown for Wan (4s) model across different methods (in 10^{15} FLOPs).

Method	Spatial	Cross	MLP
Original	13.0573	0.2816	3.0033
Delta-DiT	10.4458	0.2252	2.4026
ToCa 0.8	6.9204	0.1492	1.8741
ToCa 0.85	6.9204	0.1492	1.8035
PAB 246	8.4872	0.1173	3.0033
PAB 579	5.7452	0.1064	3.0033
Ours 0.5	6.5286	0.1408	1.5016
Ours 0.7	9.1401	0.1971	2.1023
Ours 0.4	5.2229	0.1126	1.2013